JOURNAL OF SOLID STATE CHEMISTRY 86, 75–81 (1990)

# Local Structure and Spin State of $Co^{4+}$ Ions in the Perovskite-Type $SrCo_{1-x}Mn_xO_3$ Solid–Solution

AKIRA YOSHIASA,[1] YUKARI INOUE, AND FUMIKAZU KANAMARU

*The Institute of Scientific and Industrial Research, Osaka University, Mihogaoka, Ibaraki, Osaka 567, Japan*

AND KICHIRO KOTO

*Faculty of Integrated Arts and Sciences, Tokushima University, Minami-Josanjima, Tokushima 770, Japan*

Received November 28, 1988; in revised form October 25, 1989

The local structure of the perovskite-type $SrCo_{1-x}Mn_xO_3$ solid–solution was investigated in order to study the effect of replacement of $Co^{4+}$ ions with $Mn^{4+}$ ions on the spin state of $Co^{4+}$ ion. The actual distances from $Co^{4+}$ or $Mn^{4+}$ ions to the first nearest-neighbors in the solid–solution, $R$[Co–O] and $R$[Mn–O], are determined by EXAFS method. $R$[Mn–O] decreases with increase of $Co^{4+}$ ion content in the range $0.33 \leq x \leq 1.0$ even though the lattice constant increases with $Co^{4+}$ ion content. On the other hand, $R$[Co–O] increases with $Mn^{4+}$ ion content with a break at $x = 0.33$. A lever rule is well satisfied: $(1 - x) \cdot R[\text{Co–O}] + x \cdot R[\text{Mn–O}] = R[(Co_{1-x}Mn_x)\text{–O}]$, where $R[(Co_{1-x}Mn_x)\text{–O}]$ is the mean (Co,Mn)–O distance by X-ray diffraction. These results indicate that the $O^{2-}$ ion moves toward the $Mn^{4+}$ ion and away from the $Co^{4+}$ ion in the Co–O–Mn combination. The strength of the ligand field for the $Co^{4+}$ ion becomes weak gradually with increase of $Mn^{4+}$ ion content because the $O^{2-}$ ions around $Co^{4+}$ ions are more strongly attracted to $Mn^{4+}$ ions. Little change in $R$[Mn–O] in the range $0.0 \leq x < 0.33$ can be interpreted by forming little Mn–O–Mn combinations (i.e., the Co–O–Mn and Co–O–Co combinations preferentially exist). It is proposed that the strength of the ligand field decreases sufficiently, when four of six Co–O bonds in $CoO_6$ octahedra are lengthened at the composition of $x = 0.33$, so that the spin state of $Co^{4+}$ ion changes from low to high. 

## Introduction

Transition metal oxides with the perovskite-type structure have been studied extensively. Functional properties such as catalytic activity and superconductivity have been found in the perovskite-type and its related solid–solutions.

The cubic perovskite-type oxides with the chemical formula $A^{2+}B^{4+}O_3$ ($A$ = alkaline earth ions, $B$ = transition metal ions) stabilize the tetravalent state of the first-row transition metal ions such as $Mn^{4+}$, $Fe^{4+}$, and $Co^{4+}$ under ambient conditions though these transition metal ions are normally in a divalent or trivalent state and a higher valence state is, in general, stabilized under strongly oxidizing conditions (*1–3*). The perovskite-type oxides containing transition metal ions in tetravalent state show interesting electrical and magnetic properties. The $Co^{4+}$ ion in $SrCoO_3$ is in the low spin state with $[d\varepsilon]^5[d\gamma]^0$ electron con-

[1] Present address: Faculty of Science, Hiroshima University, Hiroshima 730, Japan.



0022-4596/90 $3.00

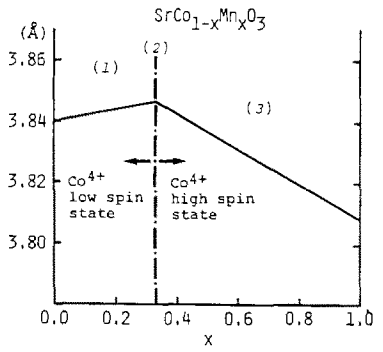


FIG. 1. The perovskite-type structure for compounds $ABO_3$.

figuration, while the $Mn^{4+}$ ion in $SrMnO_3$ takes the spin state with the $[d\varepsilon]^3[d\gamma]^0$ electron configuration. It is known by measurements of the electric resistance that $SrMnO_3$ is not conductive in contrast to the case of $SrFeO_3$ and $SrCoO_3$ (*1*). $SrCoO_3$ is a ferromagnet with Curie temperature of 222 K (*3*) and $SrMnO_3$ is an antiferromagnet with Néel temperature of 260 K (*1*).

The cubic perovskite-type oxides containing first-row transition metal, $SrMnO_3$ and $SrCoO_3$, have generally been obtained by treating the corresponding oxygen-deficient phases under high oxygen pressures at suitable temperatures, and the relation between the annealing condition under high oxygen pressures and the oxygen deficiency of samples was investigated (*1, 3*).

In the system of $SrCo_{1-x}Mn_xO_3$, the solid–solution is formed over whole composition range with the cubic perovskite-type structure (*4, 5*). The magnetic properties of the solid–solutions were investigated by Taguchi *et al.* (*3–5*). The change from ferromagnetism to antiferromagnetism occurred at about $x = 0.33$ in the system. The Curie temperature decreased with increasing $x$ in the ferromagnetic region. The Néel temperature increased with increasing $x$ in the antiferromagnetic region. The change from ferromagnetism to antiferromagnetism was attributed to a change of spin state of $Co^{4+}$ ions located at the octahedral sites. The spin state of $Co^{4+}$ ion changes from low ($[d\varepsilon]^5[d\gamma]^0$) to high ($[d\varepsilon]^3[d\gamma]^2$) at about $x = 0.33$ in connection with a peculiar variation of the lattice constants (Fig. 1). The variation of the lattice constants in the range does not follow Vegard's law. It is also interesting to note that the $Co^{4+}$ ion takes the high spin state in the range $0.33 \leq x < 1.0$ where the unit cell volume of the solid–solution is smaller than that of the solid–solution with $0.0 \leq x < 0.33$.

Figure 2 shows the cubic perovskite-type structure. $Sr^{2+}$ ions occupy the cube centers and both $Mn^{4+}$ and $Co^{4+}$ ions occupy statistically the octahedral sites. In the $SrCo_{1-x}Mn_xO_3$ solid–solution, it is expected that the local environments of the $Co^{4+}$ ions (e.g., the bond distances to the $O^{2-}$ ions) differ from those of the $Mn^{4+}$ ions. Positionally averaged information for the environments of both ions is obtained by the diffraction methods because the $Co^{4+}$ and $Mn^{4+}$ ions occupy the crystallographically equivalent positions. Extended X-ray absorption fine structure (EXAFS) spectroscopy is a useful probe of the local environment around a particular kind of absorbing atom in the solid–solution.

This work presents an EXAFS structure analysis of the solid–solution in order to study the effect of replacement of $Co^{4+}$ ions with $Mn^{4+}$ ions on the spin state of $Co^{4+}$

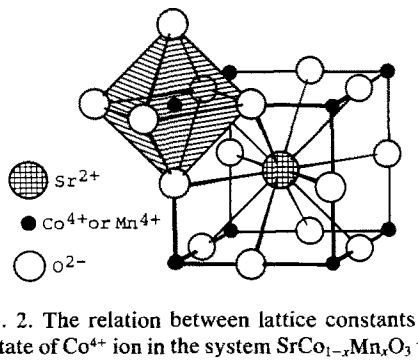


FIG. 2. The relation between lattice constants and spin state of $Co^{4+}$ ion in the system $SrCo_{1-x}Mn_xO_3$ with the cubic perovskite-type structure.

ions. The local structure and chemical bond in the solid–solution are discussed. The peculiar variation of the lattice constants is also elucidated based on the local structure.

## Experimental

### *Synthesis*

The starting materials of $MnCO_3$, basic $CoCO_3$, and $SrCO_3$ (Koso Chem. Co., Ltd.) in powder form, where the cobalt content of the basic $CoCO_3$ was determined by a chelatemetry, were weighed in the desired ratio and milled for 24 hr with acetone. The well-blended mixtures of raw materials were fired under the appropriate conditions according to the previous studies (*1*, *3–5*); after drying, the mixtures were prefired at 800°C for 24 hr, then they were reground and fired at various temperatures (1000–1350°C) for 24 hr. This firing was repeated three times for each sample. As the compounds obtained in this way were oxygen-deficient, they were annealed under oxygen pressure of 130 MPa at 300°C for 72 hr. High oxygen pressure was produced by heating an autoclave which had been cooled down to liquid nitrogen temperature and in which oxygen gas had been condensed into liquid. The formation of single phase solid–solution was confirmed by X-ray diffractometry. The lattice constants (Table I) agree excellently to the published values.

### *X-Ray Absorption Measurement*

For X-ray absorption measurements the well-ground powder samples were mixed with boron nitride in an agate mortar and pressed into pellets ~0.7 mm in thickness and 10.0 mm in diameter.

The X-ray absorption measurements near the Co K- and Mn K-edges were made with synchrotron radiation by use of the EXAFS facilities installed at the beam line 10B of the 2.5-GeV storage ring of Photon Factory in KEK, Tsukuba. Gas mixture in the ion chamber detector was selected for optimum signal to noise ratio. The spectra were observed from 7.460 to 8.710 keV for the Co K-edge and from 6.280 to 7.550 keV for the Mn K-edge. The survey regions and scanning steps of X-ray energy are shown in Table II.

TABLE I

UNIT CELL PARAMETERS ($a$) AND BOND DISTANCES ($R$) IN Å FOR THE $SrCo_{1-x}Mn_xO_3$ SOLID–SOLUTION

| | $a$ | $R$[(Co, Mn)–O] |
|---|---|---|
| $SrCoO_3$ | 3.840(1) | 1.920 |
| $SrCo_{0.95}Mn_{0.05}O_3$ | 3.838(1) | 1.919 |
| $SrCo_{0.90}Mn_{0.10}O_3$ | 3.843(1) | 1.922 |
| $SrCo_{0.85}Mn_{0.15}O_3$ | 3.847(1) | 1.924 |
| $SrCo_{0.75}Mn_{0.25}O_3$ | 3.846(1) | 1.923 |
| $SrCo_{0.70}Mn_{0.30}O_3$ | 3.847(1) | 1.924 |
| $SrCo_{0.60}Mn_{0.40}O_3$ | 3.842(1) | 1.921 |
| $SrCo_{0.50}Mn_{0.50}O_3$ | 3.838(1) | 1.919 |
| $SrCo_{0.35}Mn_{0.65}O_3$ | 3.832(1) | 1.916 |
| $SrCo_{0.20}Mn_{0.80}O_3$ | 3.826(2) | 1.913 |
| $SrCo_{0.10}Mn_{0.90}O_3$ | 3.814(1) | 1.907 |
| $SrMnO_3$ | 3.808(1) | 1.904 |

*Note.* $R$[(Co, Mn)–O] = $a/2$.

### *EXAFS Data Analysis*

EXAFS data analyses were carried out using the programs EXAFS and CURFIT

TABLE II

SURVEY REGIONS AND SCANNING STEPS OF X-RAY ABSORPTION SPECTRA IN Co K-EDGE (a) AND Mn K-EDGE (b)

| (a) Co K-edge | |
|---|---|
| 7.460–7.680 (keV) | 5.1 (eV) |
| 7.680–7.790 | 0.6 |
| 7.790–8.250 | 2.7 |
| 8.250–8.710 | 4.2 |
| **(b) Mn K-edge** | |
| 6.280–6.500 (keV) | 4.6 (eV) |
| 6.500–6.620 | 0.6 |
| 6.620–7.100 | 2.7 |
| 7.100–7.550 | 4.3 |

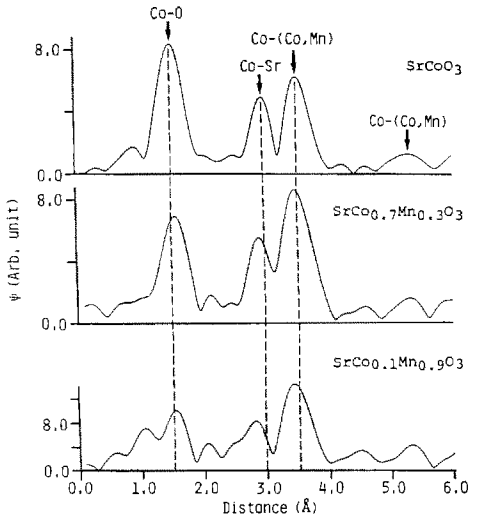


FIG. 3. Fourier transforms for the Co K-edge of $SrCo_{1-x}Mn_xO_3$ solid–solutions ($x$ = 0.0, 0.3, and 0.9). No phase shift corrections were made.

(*6*). In obtaining the EXAFS function $\chi(k)$, the background level was subtracted from the observed absorption spectra by using Victoreen fit and the absorption spectrum for the isolated atom was approximated by the cubic spline technique. The Fourier transform of $\chi(k)$ to the real space yields a radial structure function $\psi(r)$ (*7*). The Fourier transforms of $k^3$-weighted Co K- and Mn K-edge EXAFS for the solid–solutions are shown in Figs. 3 and 4, respectively, where no phase shift corrections are made.

For the purpose of curve-fitting, the distance range of interest for $\psi(r)$ was filtered with a smooth filtering window, and transformed back to $k$-space, $\chi'(k)$. Carrying out the nonlinear least-squares program of Marquardt's method (*8*), $\chi'(k)$ was fitted with analytical EXAFS function $\chi(k)$:

$$\chi(k) = \Sigma_j N_j/(kR_j^2)|f_j(\pi, k)|\exp[-2\sigma_j^2k^2] \times \exp[-2R_j/\lambda(k)]\sin[2kR_j + \Phi_{ij}(k)].$$

Here $N_j$ is the number of atoms in the $j$-th shell at distance $R_j$; $|f_j(\pi, k)|$, the back-scattering amplitude; $\sigma j$, the Debye–Waller factor; $\exp[-2R_j/\lambda_j(k)]$, the damping factor due to inelastic losses in the scattering process with the electron mean free path $\lambda_j(k)$; and $\Phi_{ij}(k)$, the phase shift experienced by the photoelectron. The back-scattering amplitude $|f_j(\pi, k)|$ and the phase shift $\Phi_{ij}(k)$ are parameterized as follows (*9*, *10*),

$$|f_j(\pi, k)| = A_j/(1 + B_j^2(k - C_j)^2$$
$$\Phi_{ij}(k) = a_j + b_jk + c_jk^2 + d_j/k^3$$
$$k = [k'^2 - 0.2625(\Delta E_0)]^{1/2},$$

where $k'$ and $\Delta E_0$ are the experimental wave number of photoelectron and the difference in energy threshold between theory and experiment, respectively. The parameters in the $j$-th shell $[A_j, B_j, C_j]$, $[a_j, b_j, c_j, d_j]$ determined from each end-member (pure $SrCoO_3$ and $SrMnO_3$) as the reference sample were fixed through the refinements

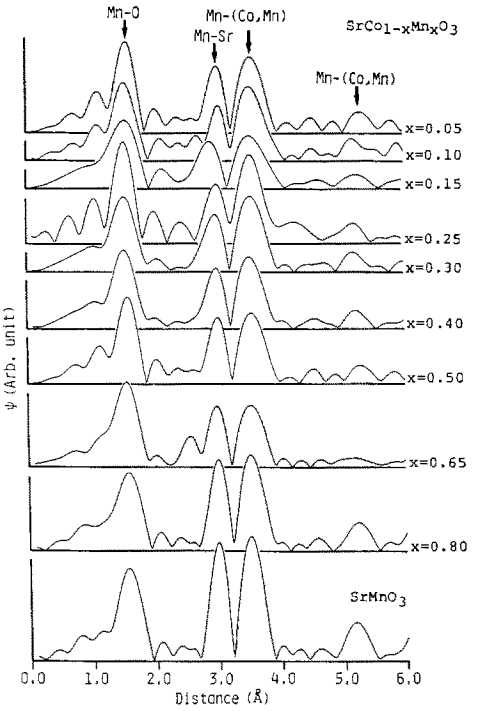


FIG. 4. Fourier transforms for the Mn K-edge of $SrCo_{1-x}Mn_xO_3$ solid–solutions. No phase shift corrections were made.

for the solid–solutions. The refinements were applied to $\Delta E_0$ and three structure parameters, $N_j$, $R_j$, and $\sigma_j$. The structure parameters of first shells for each solid–solution determined by the least-squares parameter fitting are listed in Table III. The reliability of fit parameter, $R = \Sigma_s|k_s^3\chi(k_s)\text{expt.} - k_s^3\chi(k_s)\text{calcd.}|/\Sigma_s|k_s^3\chi(k_s)\text{expt.}|$, between the experimental and calculated EXAFS function is also listed in Table III. The errors quoted in Table III were estimated from statistical fitting errors and are given only for reference. It should be considered that the relative comparison of the results determined by each end-member using analytical EXAFS formula of the plane-wave approximation provides sufficient precision to prove the local structure in the solid–solution.

TABLE III

STRUCTURE PARAMETERS DETERMINED BY THE LEAST-SQUARES PARAMETER FITTING

| | Co K-edge | | | |
|---|---|---|---|---|
| | $N$[Co–O] | $R$[Co–O] | $\sigma$(Co–O] | $R$-factor |
| $SrCoO_3$ | 6* | 1.920* | 0.10(1) | |
| $SrCo_{0.90}Mn_{0.10}O_3$ | 6(2) | 1.926(3) | 0.11(1) | 0.17% |
| $SrCo_{0.85}Mn_{0.15}O_3$ | 7(2) | 1.929(4) | 0.11(1) | 0.16% |
| $SrCo_{0.70}Mn_{0.30}O_3$ | 5(2) | 1.942(4) | 0.10(1) | 0.19% |
| $SrCo_{0.60}Mn_{0.40}O_3$ | 4(3) | 1.944(7) | 0.10(1) | 0.20% |
| $SrCo_{0.50}Mn_{0.50}O_3$ | 4(3) | 1.937(7) | 0.09(1) | 0.29% |
| $SrCo_{0.20}Mn_{0.80}O_3$ | 6(1) | 1.947(4) | 0.11(1) | 0.11% |
| $SrCo_{0.10}Mn_{0.90}O_3$ | 7(1) | 1.944(4) | 0.10(1) | 0.64% |
| | Mn K-edge | | | |
| | $N$[Mn–O] | $R$[Mn–O] | $\sigma$[Mn–O] | $R$-factor |
| $SrCo_{0.95}Mn_{0.05}O_3$ | 6(1) | 1.889(3) | 0.12(1) | 1.95% |
| $SrCo_{0.90}Mn_{0.10}O_3$ | 6(1) | 1.887(4) | 0.11(1) | 1.72% |
| $SrCo_{0.85}Mn_{0.15}O_3$ | 6(1) | 1.892(4) | 0.12(1) | 2.04% |
| $SrCo_{0.75}Mn_{0.25}O_3$ | 7(1) | 1.889(4) | 0.11(1) | 0.35% |
| $SrCo_{0.70}Mn_{0.30}O_3$ | 6(1) | 1.892(4) | 0.11(1) | 1.33% |
| $SrCo_{0.60}Mn_{0.40}O_3$ | 6(1) | 1.891(2) | 0.11(1) | 1.46% |
| $SrCo_{0.50}Mn_{0.50}O_3$ | 6(1) | 1.892(4) | 0.11(1) | 0.41% |
| $SrCo_{0.35}Mn_{0.65}O_3$ | 6(1) | 1.896(2) | 0.11(1) | 0.39% |
| $SrCo_{0.20}Mn_{0.80}O_3$ | 6(1) | 1.900(4) | 0.12(1) | 0.41% |
| $SrMnO_3$ | 6* | 1.904* | 0.11(1) | |

*Note.* Co-ordination numbers ($N$), interatomic distances ($R$(Å)), and Debye–Waller factors ($\sigma$).

## Results and Discussion

EXAFS and XANES spectra yield information on the local environments around a particular kind of absorbing atom in the solid–solution. The photon energies of the thresholds of Co K- and Mn K-edges for the solid–solutions have constant values of 7.723 and 6.553 keV, respectively, which indicates that there is little change in valence of Co and Mn ions in the solid–solution. The features of Co K-edge XANES spectra change discontinuously at $x = 0.33$ accompanying the change of the spin state of $Co^{4+}$ ion. On the other hand, such a behavior is not observed in the Mn K-edge XANES spectra.

In both Fourier transforms of Co K- and Mn K-edge EXAFS for the solid–solutions (Figs. 3 and 4), three peaks are clearly recognized corresponding to the interatomic distances of Co–O or Mn–O (first shell), Co–Sr or Mn–Sr (second shell), and Co–(Co, Mn) or Mn–(Co, Mn) (third shell). The second and third shells decrease with Mn content in the range $0.33 \leq x \leq 1.0$. The composition dependence of Co–(Co, Mn) and Mn–(Co, Mn) distances obtained from the Fourier transforms is in accord with that of the lattice constants of the cubic perovskite-type structure.

The actual Co–O and Mn–O distances determined by the curve-fitting analyses of first shells in the solid–solutions are plotted in Fig. 5 with the mean (Co, Mn)–O distances obtained by X-ray diffraction (one-half of the lattice constant). It is revealed that the Mn–O distance decreases with increase of $Co^{4+}$ ion content in the range $0.33 \leq x \leq 1.0$ even though the lattice constant increases with $Co^{4+}$ ion content, while in the range $0.0 \leq x < 0.33$ little change in the Mn–O distance is observed. On the other hand, the Co–O distance increases with $Mn^{4+}$ ion content with a break at $x = 0.33$. In Figure 8, a lever rule is well satisfied: $(1 - x) \cdot R[\text{Co–O}] + x \cdot R[\text{Mn–O}] =$

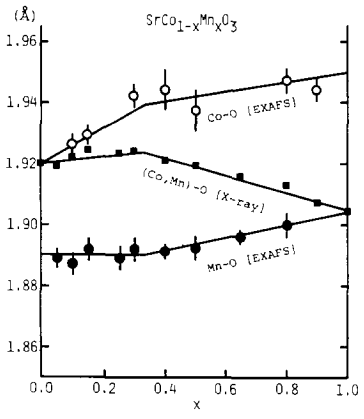


FIG. 5. The Co–O and Mn–O nearest neighbor distances measured by EXAFS and the mean (Co, Mn)–O distances by X-ray diffraction in the perovskite-type $SrCo_{1-x}Mn_xO_3$ solid–solution.

$R[(Co_{1-x}Mn_x)–O]$, where $R$[Co–O], $R$[Mn–O], and $R[(Co_{1-x}Mn_x)–O]$ are the Co–O, Mn–O, and mean (Co, Mn)–O distances, respectively.

The variations in the distances from the $Co^{4+}$ or $Mn^{4+}$ ion to the first nearest-neighbor, oxide ion, can be reasonably interpreted assuming that the $O^{2-}$ ion is more strongly attracted to the $Mn^{4+}$ ion in the Co–O–Mn combination; that is, the $O^{2-}$ ion shifts toward the $Mn^{4+}$ ion from the midpoint in the Co–O–Mn (Fig. 6). It is interesting to note that the Mn–O bonding in the perovskite-type oxides was stronger than that in manganese oxides with a different crystal structure (*4*). The similar phenomenon in a particular atom pair is observed in other systems such as the $AgBr_{1-x}I_x$ NaCl-type solid–solution (*11, 12*).

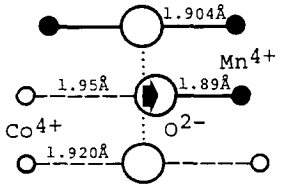


FIG. 6. The Co–O and Mn–O distances in the Co–O–Co, Co–O–Mn, and Mn–O–Mn combinations. The $O^{2-}$ ion shifts toward the $Mn^{4+}$ ion in the Co–O–Mn combination.

This idealized model must result in that the Co–O distribution becomes bimodal with a long Co–O distance corresponding to a Co–O–Mn configuration and a short distance for the Co–O–Co distribution. However, the peak separation for the first shell in radial structure functions around the Co ions is not observed because there is no sufficient difference in the Co–O distances between high spin and low spin states ($\Delta R \leq 0.03$ Å) and each distance could not be analyzed separately by simultaneous refinement of curve-fitting because of the strong correlation among the structure parameters in individual shells. The same can be applied for the first shell around the Mn ions.

In the range $0.33 \leq x \leq 1.0$, the decrease in the Mn–O distance is explained by an increase in the number of Co–O–Mn combinations with increase of $Co^{4+}$ ion content. In the range $0.0 \leq x < 0.33$, little change in Mn–O distance can be also interpreted by forming little Mn–O–Mn combination (i.e., an ordered arrangement of $Mn^{4+}$ ions, where the Co–Co–Mn and Co–O–Co combinations preferentially exist). The composition dependence of the Co–O distances is also explained by increase of Co–O distances due to the formation of Co–O–Mn combinations. The strength of the ligand field for $Co^{4+}$ ion becomes weak gradually with increase of $Mn^{4+}$ ion content because the $O^{2-}$ ions around $Co^{4+}$ ions are attracted to $Mn^{4+}$ ions. It can be, therefore, understood why larger $Co^{4+}$ ion in the high spin state is more stable than $Co^{4+}$ ion in the low spin state in the range $0.33 \leq x < 1.0$ though the solid–solutions have smaller unit cell volumes than that of $SrCo_{0.67}Mn_{0.33}O_3$ in which $Co^{4+}$ ion is in low spin state.

One of the possible atomic arrangements satisfying the ordered condition of $Mn^{4+}$ at

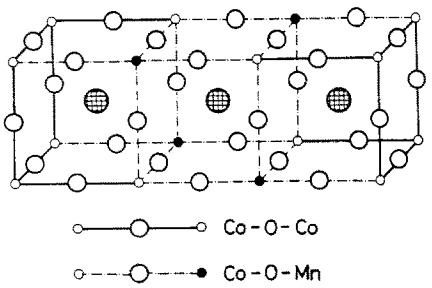


FIG. 7. One of the possible arrangements of atoms at the composition of $x = 0.33$ satisfying the ordered condition which fails to form the Mn–O–Mn combination.

the composition of $x = 0.33$ is shown in Fig. 7, where the overall composition of these three unit cells in the crystal lattice is $Sr_3Co_2Mn_1O_9$. In this arrangement the ratio of $N$[Co–O–Mn]/($N$[Co–O–Co] + $N$[Co–O–Mn]) is 6/9, where $N$[Co–O–Mn] and $N$[Co–O–Co] are the numbers of Co–O–Mn and Co–O–Co combinations, respectively. The ratio is equivalent to the proportion of the number of lengthened Co–O bonds in a $CoO_6$ octahedron. It is considered that the strength of the crystalline field at $Co^{4+}$ ions decreases sufficiently when four of six Co–O bonds in $CoO_6$ octahedra are lengthened at the composition of $x = 0.33$, resulting in the spin state of $Co^{4+}$ ion changes from low to high.

## Acknowledgments

We are grateful to Dr. H. Maeda, Okayama University, for the computer programs of EXAFS analysis and to Drs. S. Nomura and A. Koyama, the National Laboratory for High Energy Physics, KEK, for their indispensable assistance on EXAFS measurements. Discussion with and useful information from Dr. H. Taguchi, Okayama University, are much appreciated. All computations were carried out at the Crystallographic Research Center, Institute for Protein Research, Osaka University. This work has been performed under the approval of the Photon Factory Program Advisory Committee (Proposal No. 86-090). Part of the expenses for this work was defrayed by a research grant from the Ministry of Education of the Japanese Government.

## References

1. T. TAKEDA AND S. OHARA, *J. Phys. Soc. Japan* **37,** 275 (1974).
2. Y. TAKEDA, S. NAKA, M. TAKANO, T. SHINJO, T. TAKEDA, AND M. SHIMADA, *Mater. Res. Bull.* **13,** 61 (1978).
3. H. TAGUCHI, M. SHIMADA, AND M. KOIZUMI, *J. Solid State Chem.* **29,** 221 (1979).
4. H. TAGUCHI, M. SHIMADA, M. KOIZUMI, AND F. KANAMARU, *J. Solid State Chem.* **35,** 246 (1980).
5. H. TAGUCHI, M. SHIMADA, F. KANAMARU, M. KOIZUMI, AND Y. TAKEDA, *J. Solid State Chem.* **18,** 299 (1976).
6. H. MAEDA, *J. Phys. Soc. Japan* **56,** 2777 (1987).
7. E. A. STERN, D. E. SAYERS, AND F. W. LYTLE, *Phys. Rev. B* **11,** 4836 (1975).
8. D. W. MARQUARDT, *J. Soc. Ind. Appl. Math.* **11,** 431 (1963).
9. B. K. TEO, P. A. LEE, A. L. SIMONS, P. EISENBERGER, AND B. M. KINCAID, *J. Amer. Chem. Soc.* **99,** 3854 (1977).
10. P. A. LEE, B. K. TEO, AND A. L. SIMONS, *J. Amer. Chem. Soc.* **99,** 3856 (1977).
11. A. YOSHIASA, K. KOTO, S. EMURA, AND F. KANAMARU, *J. Phys. Colloq. (C8 Suppl.)* **47,** 803 (1986).
12. A. YOSHIASA, K. KOTO, S. EMURA, AND F. KANAMARU, *Solid State Ionics* **27,** 267 (1988).